A Twin-Core and Dual-Hole Fiber Design and Fabrication

Tingting Yuan , Xiaotong Zhang, Qi Xia, Yiping Wang , and Libo Yuan

Abstract—We have proposed and demonstrated novel twin-hole and dual-core optical fiber. We used the normal MCVD technology to fabricate a single core fiber preform with a thin cladding. Then, two small holes were drilled in the center and on the side of the pure silica rod, the fabricated single-core fiber preform was inserted into the two holes, and then the combined preform was heated until three parts were fused. Finally, two larger holes were drilled close the center core and twin-core and dual-hole are vertically distributed. In order to retain the shape of air hole, we filled nitrogen gas in the two holes to against the ambient pressure, which made the holes collapse during the fiber drawing. The dual-hole microstructure may be used as micro-containers to inject modulation medium and aside the center core, and to induce accumulated interaction between flow material and evanescent field of the center core, therefore, it can be used as a modulation function fiber to fabricate a very compact in-fiber integrated device.

Index Terms—Twin-core optical fiber, micro-container fiber, multifunctional sensors, in-fiber integrated device.

I. INTRODUCTION

IN-FIBER integrated device is a burgeoning field that owes to the growing awareness of new structures and new materials of optical fiber are emerging continuously, which provides a variety of possibilities for the expansion of new functions of optical fiber, such as photonic crystal fiber [1], [2], multicore fiber [3]–[5], chiral fiber [6]–[8], metamaterial fiber [9], [10] and microstructure fiber [11], [12]. Most of the optical fiber sensors are based on the same operation principle, i.e. the evanescent field sensing, and all of them make use of optical waveguides as

Tingting Yuan and Yiping Wang are with the Key Laboratory of Optoelectronic Devices and Systems of Ministry of Education and Guangdong Province, College of Optoelectronic Engineering, Shenzhen University, Shenzhen 518060, China (e-mail: ttyuan90@126.com; ypwang@szu.edu.cn).

Xiaotong Zhang and Qi Xia are with the Key Laboratory of In-Fiber Integrated Optics, Ministry Education of China, Harbin Engineering University, Harbin 150001, China (e-mail: zhangxiaotong1211@foxmail.com; xiaqi_hrb@163.com).

Libo Yuan is with the Photonics Research Center, School of Electronic Engineering and Automation, Guilin University of Electronic Technology, Guilin 541004, China (e-mail: lbyuan@vip.sina.com).

Color versions of one or more of the figures in this article are available online at https://ieeexplore.ieee.org.

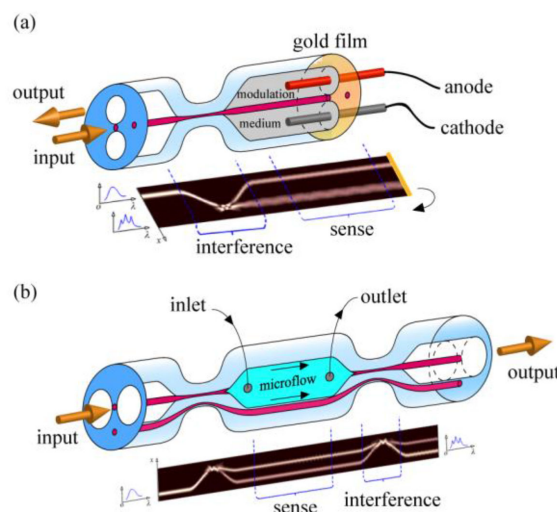Digital Object Identifier 10.1109/JLT.2020.3022104

Fig. 1. Integration devices by a specially designed functional optical fiber. (1) In-fiber integrated modulator; (2) In-fiber integrated microfluidic sensor.

the fundamental element of their structure for light propagation. For example, the Michelson interferometer or the Mach-Zehnder interferometer are most commonly employed for sensing. The evanescent wave penetration into the adjacent media is in the order of hundreds of nanometers, depending on the sensors structure, being able to interact with the environment.

As we all know, microstructure fiber with porosity have been widely used in optical fiber sensors. Hollow photonic crystal fibers can greatly improve the interaction between light and microfluidic material. However, this kind of fiber using a bandgap waveguide mechanism [13]–[15] is difficult to be applied to control the infiltration of the liquid in the bandgap structure. In addition, C. E. Kerbage *et al.* reported a six-hole optical fiber around a central fiber core [16], but the interaction between light and matter is weakened due to the large distance between the fiber core and the microflow in the hole. On the other hand, because the fiber has only one core, it is difficult to construct a double-path interferometer on the same fiber.

In order to overcome the above shortcomings, we propose to build-up an in-fiber integrated component in the optical fiber, which has a microporous structure, and also includes a dual waveguide as an interferometer, so that one beam is used as a reference, and the other as a modulation or sensing, as shown in Fig. 1.

If we have this kind of fiber, then the microsensors "Lab-in-a-fiber" may be easy to fabricate. The schematic diagram of
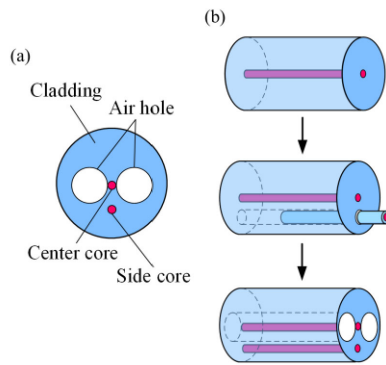
Fig. 2. (a) The schematic diagram of the twin-core optical fiber with a dual-hole; (b) Fabrication process of the microstructure optical fiber preform: firstly, a single core fiber preform; secondly, a twin-core preform; and thirdly, drill two air holes near the central core in the twin-core preform.

Fig. 3. The drawing process of fiber with twin-core and dual-hole.

optical fiber modulator is shown in Fig. 1(a), this fiber is used to prepare a Michelson interferometer, and the air holes structure is used as a microcontainer for the modulation medium. Fill the hole with the medium having the characteristics of electro-optic effect or magneto-optic effect as a modulation medium (for example, electro-optic crystal, graphene, magneticfluid). Due to the high adjust coefficient of the medium, when the voltage, magnetic field or other control parameters change, the refractive index (RI) of the medium will also change, thereby realizing the modulation function of the sensor [17]–[20]. Fig. 1(b) is a Mach-Zehnder interferometer optofluidic sensor prepared by using this fiber. Unlike the previous devices, this sensor naturally forms a microcavity because of the structure of the Mach-Zehnder interferometer. The micro-processing of the microcavity can make solutions of different RI flow in and out. The change of the liquid in the air holes can be monitored through spectroscopy, which is always a dynamic process.

Therefore, in this work, a novel type of microstructured optical fiber with twin-core and dual-hole is proposed, which is very suitable for use as an integrating interferometer microsensor. Since the center core is located close to the air hole, the evanescent wave in the core will interact with the medium, which makes the core sensitive to changes in the refractive index of the material in the holes, therefore achieving the purpose of modulating the output optical signal. Integrated optics technology can combine the waveguide and the microcontainer in one optical fiber, so that miniaturized compact sensing devices can be flexibly developed, and optical integrated devices can be fabricated in a single optical fiber.

II. DESIGN AND FABRICATION OF THE FIBER PREFORM

Fig. 2(a) shows a schematic diagram of a novel microstructured optical fiber with dual-hole and twin-core designed by us. The size of the side core is the same as the center core. Both air holes are very close to the center core, and are located on the same horizontal line, so this new microstructure is suitable for fiber-optic modulation sensors. The sensor has two optical paths and two microcontainers to accommodate the modulation medium, the cen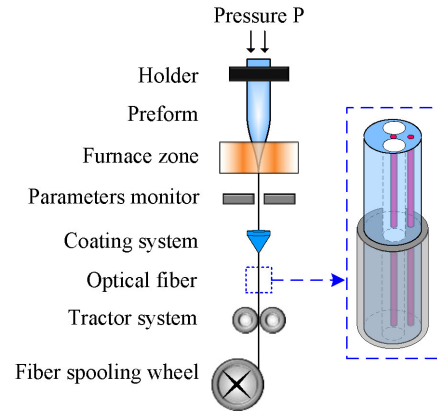ter core near the holes is used as the detection path and the side core away from the center core is used as the reference path. The material in the hole will interact strongly with the central core, but it will not affect the side core.

The fiber structure proposed in this paper is different from the traditional single-core optical fiber preform. Firstly, use the traditional modified chemical vapor deposition (MCVD) technology to manufacture a standard single-core fiber preform. Then, drill a small hole near the single core of the single-core fiber preform, and insert a thin-clad core preform into this small hole. Next, heat and melt the two in a vacuum to exhaust the air in the gap until the preforms are combined. Finally, drill two atmospheric holes near the central core of the preform, and a dual-core optical fiber preform with two air holes is obtained. This fabrication process of the twin-core and dual-hole fiber preform is shown in Fig. 2(b).

III. DRAWING THE FIBER WITH DUAL-CORE AND A SIDE-HOLE

The preparation steps of the microstructured optical fiber are similar to the conventional single-core standard optical fiber. After the optical fiber preform is prepared, heat it to a high temperature in the drawing tower. When the preform is melted and sufficient to flow, a drop of molten preform is pulled from the bottom of the furnace, then a coating is applied on the outside of the silica fiber, and it is wound up by the traction machine. The constant speed of the reel can ensure that the fiber diameter is stable, and the fiber will be measured through the parameter monitor. Since the microstructured optical fiber preform has air holes, in order to avoid the collapse of the air holes during the drawing process, an immobile nitrogen pressure needs to be added at the upper end of the preform to balance the pressure inside and outside the air holes. The drawing process is shown in Fig. 3, although the manufactured optical fiber has two air holes, it can still achieve the same robustness and physical matching size as the standard optical fiber. Generally, the temperature range is controlled to be between 1900 and 2000 °C, and nitrogen gas is pumped into the holes and is maintained at a pressure greater than that of the outside atmosphere. In our experiment, the furnace temperature was controlled to be at 1950 °C, and the
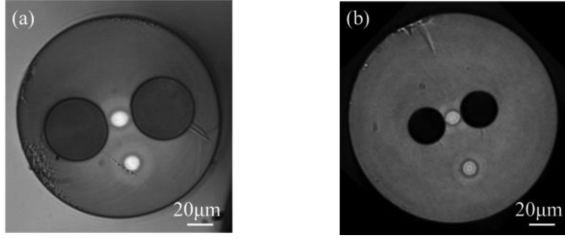
Fig. 4. Cross-section view photograph of the fiber sample with twin-core and dual-hole: (a) sample 1; (b) sample 2.
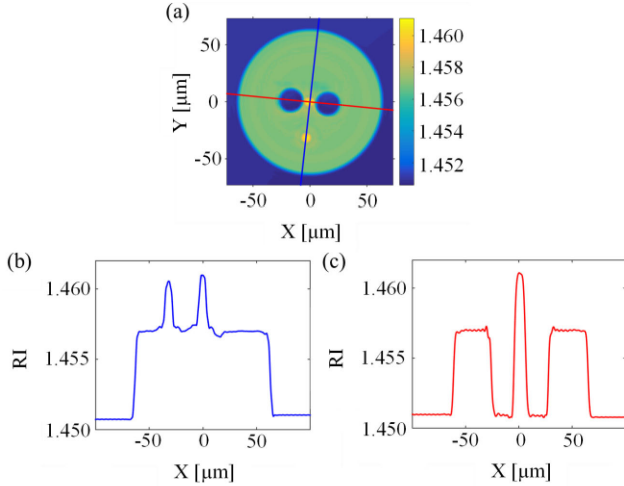

Fig. 5. RI profile of the fiber sample 2: (a) RI diagram of fiber end face; (b) RI data in the blue line; (c) RI data in the red line.

nitrogen pressure was set at 101.345 kp at a drawing speed of 150 m/ min.

IV. CHARACTERISTICS OF THE FIBER WITH DUAL-CORE AND A SIDE-HOLE

A. Optical Fiber Samples and the Refractive Index Profile

Compared with single-hole fibers, the double-hole structure has many new advantages, such as expanded functions, improvements of the sensing sensitivity, increase of the types of substances that can be measured, and so on. Here we prepared these two kinds of optical fiber samples with the same structure but different sizes. The outer diameters of both samples are 125 μm, the air hole diameter of sample 1 (Fig. 4a) is 38 μm, the diameters of the center core and the side core are 9.1 μm, and the distance between the two cores is 28.4 μm; the air hole diameter of sample 2 (Fig. 4b) is 22.1 μm, the diameters of the two cores are 8 μm, and the distance between the two cores is 31.8 μm. We can observe the cross-sections of the two microstructured fiber samples through a microscope and measure their specific dimensions.

As can be seen in Fig. 5, the RI distribution of the fiber sample is measured by RI profiler. The core and cladding RI of sample 1 and sample 2 are 1.462 and 1.457, respectively.
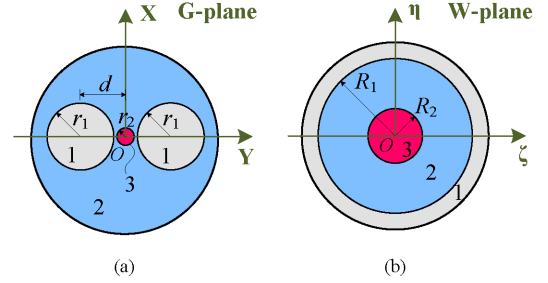

Fig. 6. The conformal transformation for the dual-hole fiber. (a) Cross-section of the eccentric air hole fiber on the G-plane. (b) The concentric circles mapped on the W-plane.

B. Waveguide Mode Field Characteristics of Adjacent Microflow Holes

Base on the mapping technique, the fiber with dual-hole could be transformed into a four layers structure from the G-plane to the W-plane, as shown in Figs. 6(a) and 6(b). Although the geometry after conformal transformation is simplified, the Helmholtz wave equation is not easy to solve [21]. We set the G plane as the plane before the conformal transformation, and we set the W plane as the plane after the transformation (Fig. 6), based on the mapping technique [22], the Helmholtz wave equation becomes the following equation:

$$[\nabla^2 + (k^2 n^2 - \beta^2)/|W'(G)|^2]\mathbf{E} = 0 \tag{1}$$

Here $W'(G) = \mathrm{d}W/\mathrm{d}G$.

If the above problems can be solved, then this mapping technique can be considered reasonable [23]. The conversion relationship between the G plane and the W plane can be described as

$$W(G) = -s\frac{z-t}{z-s} \quad (L > 0, s < t < 0) \tag{2}$$

In Eq. (2), s and t are the roots of the following equations

$$\begin{cases} st = r_2^2 \\ (s+L)(t+L) = r_1^2 \end{cases} \tag{3}$$

R_1 and R_2 are the radiuses of the inner and the outer circles respectively in the W-plane. Assuming $R_1 = r_1$, Eq. (2) can be rewritten as

$$z = \frac{Ws + st}{W + s} \tag{4}$$

If $W = r\exp(j\varphi)$, we obtain

$$1/|W'(z)| = \left| \frac{1 - t/s}{1 + 2r\exp(j\varphi)/s + r^2/s^2} \right| \tag{5}$$

From Eq. (5), $1/|W'(G)|^2$ can expand into a series of power r/s:

$$1/|W'(G)|^2 = \left(1 - \frac{t}{s}\right)^2 / \left(1 + \frac{4r\cos\varphi}{s} + L\right) \tag{6}$$
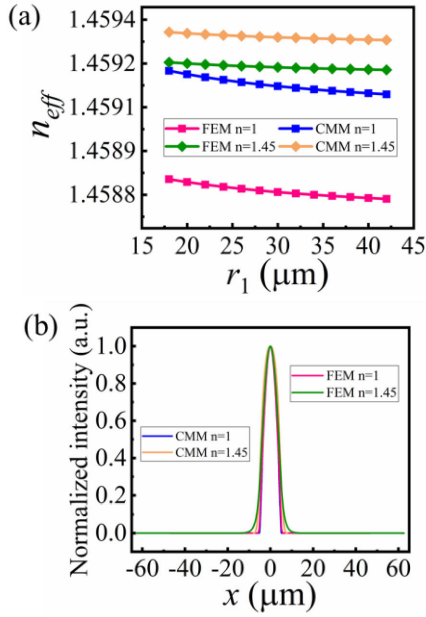
Fig. 7. The difference between FEM and CMM. (a) The relationship between the effective RI of the center core and the hole size when the eccentric stomatal fiber has a modulation medium or not. (b) The electric field mode distribution in air and medium in the same Cartesian coordinate system, respectively in air and water.

If $L + s$ is great enough, the term $4r \cos \varphi/(L + s)$ can be absolutely negligible (<1%) [24]. Thus, the zero-order approximation of Eq. (1) can be expressed as follow:

$$\left[\nabla^2 + \left(1 - \frac{t}{s}\right)^2 (k^2 n^2 - \beta^2)\right] \mathbf{E} = 0 \tag{7}$$

Based on Eq. (7), the longitudinal field components can be written as

$$E_z =$$
$$\begin{cases} AJ_m(u_1 r/R_2)\cos(m\varphi) & r < R_2 \\ [BI_m(u_2 r/R_2) + CK_m(u_2 r/R_2)]\cos(m\varphi) & R_2 < r < R_1 \\ DK_m(u_3 r/R_1)\cos(m\varphi) & r > R_1 \end{cases}, \tag{8}$$

Here, J_m is the mth order Bessel function of the first kind, I_m and K_m are the mth order modified Bessel functions of the first kind and the second kind, respectively. The constant Eqs. (8) should be determined by the continuous condition of the tangent component at the boundary. As a result, just like the traditional three-layer fiber, by using these phase parameters to solve the corresponding characteristic equations, the propagation constant of the mode propagating in our fiber can also be calculated [25].

Compared with finite element modeling (FEM), conformal mapping method (CMM) has been proved to be an effective and direct solution for optimizing eccentric structured fibers with fewer errors. When the air holes are 43 μm in a 1500 nm wavelength and $d = 26.5$ μm, Fig. 7(a) plots the effective RI of the fundamental mode of the central core with different air holes sizes. It is worth noting that a decrease in the difference

of effective RI between FEM and CMM is accompanied by an increase in the RI of the medium in the holes. When $n_1 = 1$, The maximum difference is 3.35×10^{-4} and when $n_1 = 1.45$, the maximum difference is only 9.55×10^{-5}, so it is proved that this method is suitable for solving eccentric structured fibers.

The field distributions of the fundamental mode of the central core on the W plane and G plane are shown in Fig. 7(b). In the simulation, the proposed method was evaluated by the measuring parameters $n_1 = 1$ or $n_1 = 1.45$, $n_2 = 1.457$, $n_3 = 1.462$ in fiber samples. Since the structure of the air holes area are bilaterally symmetric, the distribution of the waveguide model in the center core is still a gaussian at the origin. The simplified structure after conformal transformation is similar to a single-mode fiber, so the distribution of the waveguide model should also be at the origin. However, there is still a difference between FEM and CMM in the simplified geometry. In order to solve the position deviation problem introduced by CMM, when it is inversely transformed back to the original coordinate system, we perform a second conformal transformation on the structure, following formula:

$$\begin{aligned} Z &= \alpha(Z - t) \\ \alpha &= r_2/(r_2 + t), t < 0 \\ \alpha &= r_2/(r_2 - t), t > 0 \end{aligned} \tag{9}$$

In fact, the numerical results and analytical solutions are approximates, so they all have error bands. At the same time, their difference is not enough to affect our comparative analysis, as can be seen from Fig. 6(b), there is not much difference between FEM and CMM, the difference is small and can be ignored. Based on these data, it is proved that this method is suitable for the solution of double-hole structured optical fiber, and the accuracy of this method is proved.

C. Interaction Between Fluidic Materials and Evanescent Optical Field of the Center Core

By using finite element software, it is possible to simulate the effective RI of the fiber's central core mode at different wavelengths. Fig. 8(a) is the central core effective RI of the dual-hole and twin-core optical fiber with air holes of a diameter of 22 μm at different wavelengths. Due to the change in the RI of the modulation medium in the air holes, the effective RI of the central core mode will also change. Since the positions of the central core and the holes are almost tangent, the change of the evanescent field in the core will sensitively transform with the alteration of the RI of the medium in the holes. We found that as the RI of the material in the hole increases, the effective RI of the core also increases.

The proportion of the evanescent field of light waves in the air hole is considered to be able to assess the sensitivity of the sensor. In the case of injecting different RI modulation medium into the hole, the energy ratio of the energy in the hole to the total energy at different wavelengths is analyzed. The energy ratio in the fiber is defined as $\eta = P_{\text{hole}}/P_{\text{total}}$, where P_{hole} represents the optical power in the air holes, and P_{total} is the total power of the entire area. The power ratio η between the stomata and the entire area is shown in Fig. 8(b). As the wavelength increases, the van evanescent field in the hole will increase as the medium
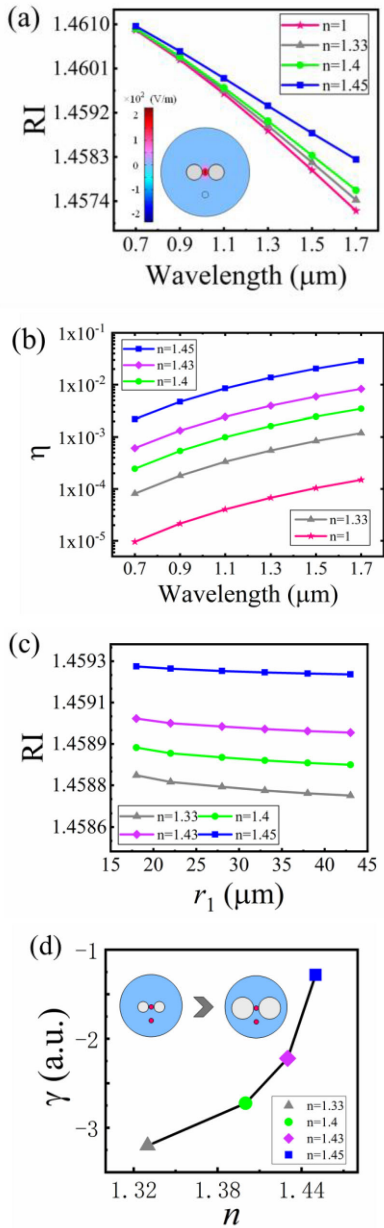
Fig. 8. (a) The effect of different materials on the effective RI of the central core, insert: simulation results of evanescent field distribution with air in the air hole. (b) The power ratio of the evanescent wave in the air hole of the fiber which filled in different materials. (c) The relationship between the effective RI of the center core and the hole size with different modulation medium. (d) The relationship between modulation medium and γ which is the holes size affects the n_{eff} of the center core ratio.

RI increases. The above data graphic was obtained when the air holes had diameters of 22 μm in a 1500 nm wavelength. Although, the size of the holes also affect the performance of the fiber, but from Fig. 8(c) we found that the relationship between the two is not obvious and the effective refractive index of the central core tends to be flattened as the hole increases. γ is the linear fitting slope of each data line in Fig. 8(c), expressed as the degree to which the holes size affects the effective RI of the center core. It can be seen from Fig. 8(d) that γ will become

larger when the RI of the modulation medium in the hole become larger, that is, the larger the RI of the medium, the smaller the effect of the hole size on the core (Fig. 8d).

Since the center core is obviously affected by the material in the holes, but the side core is not, because they are far enough away from each other that they do not interfere with each other, so it has the potential to be an optical interference sensor. In addition, the characteristics of low consumption and high sensitivity are suitable for interference microstructured sensors. These advantages have attracted considerable attention in the use of fiber optic sensing.

This new microstructured optical fiber with twin-core and dual-hole has advantages such as a micro-size, tracing of sample measurement, material control in the microholes, and a stable environment. In addition to this, there are other superiorities, for example, in this integrated optical paths, the light wave can be easily transmitted over long distances, and clear results can be obtained in a low-key range. The device combines material and light, and the optical propagation path of the core will be affected by the modulation medium RI in the microholes. The optical signal can reflect certain characteristics of the detected electromagnetic field.

V. CONCLUSION

A novel type of microstructured optical fiber, which integrates the micro-container and the optical waveguide into one optical fiber, has been designed and fabricated. We proposed that the eccentric construction can be transformed into a concentric optical fiber through the CMM. The CMM is used to simplify the dual-hole structure, and the corresponding light field distribution is obtained. For sensing application, the in-fiber multifunction integrated device has a low loss, a fast response and a high sensitivity. In-fiber integrated technology allows the integration of passive and active optical components into a single fiber, allowing the flexible development of miniaturized compact sensing devices, with the additional possibility to fabricate multifunctional sensors inside one fiber. The in-fiber integration technology offers some additional advantages to the optical sensing systems, such as robustness, reliability, potential for mass production with consequent reduction of production costs, low energy consumption and simplicity in the alignment of the individual optical elements.

REFERENCES

[1] P. S. J. Russell, "Photonic-crystal fibers," *J. Lightw. Technol.*, vol. 24, no. 12, pp. 4729–4749, 2006.
[2] J. C. Knight, T. A. Birks, P. S. J. Russell, and J. P. de Sandro, "Properties of photonic crystal fiber and the effective index model," *J. Opt. Soc. Amer. A*, vol. 15, no. 3, pp. 748–752, 1998.
[3] K. Saitoh and S. Matsuo, "Multicore fibers for large capacity transmission," *Nanophotonics*, vol. 2, nos. 5/6, pp. 441–454, 2013.
[4] X. Zhang *et al.*, "In-fiber integrated optics: An emerging photonics integration technology [Invited]," *Chin. Opt. Lett.*, vol. 16, no. 11, 2018, Art. no. 110601.
[5] T. Hayashi, T. Taru, O. Shimakawa, T. Sasaki, and E. Sasaoka, "Design and fabrication of ultra-low crosstalk and low-loss multi-core fiber," *Opt. Express*, vol. 19, no. 17, pp. 16576–16592, 2011.
[6] V. I. Kopp and A. Z. Genack, "Adding twist," *Nature Photon.*, vol. 5, no. 8, pp. 470–472, 2011.

[7] V. I. Kopp, J. Park, M. Wlodawski, J. Singer, D. Neugroschl, and A. Z. Genack, "Chiral fibers: Microformed optical waveguides for polarization control, sensing, coupling, amplification, and switching," *J. Lightw. Technol.*, vol. 32, no. 4, pp. 605–613, 2014.

[8] R. C. Qiu and I. T. Lu, "Guided waves in chiral optical fibers," *J. Opt. Soc. Amer. A*, vol. 11, no. 12, pp. 3212–3219, 1994.

[9] S. Atakaramians, A. Argyros, S. C. Fleming, and B. T. Kuhlmey, "Hollow-core uniaxial metamaterial clad fibers with dispersive metamaterials," *J. Opt. Soc. Amer. B*, vol. 30, no. 4, pp. 851–867, 2013.

[10] D. Pratap, S. Anantha Ramakrishna, J. G. Pollock, and A. K. Iyer, "Anisotropic metamaterial optical fibers," *Opt. Express*, vol. 23, no. 7, pp. 9074–9085, 2015.

[11] J. Yang *et al.*, "High sensitivity temperature sensor based on liquid filled hole-assisted dual-core fiber," *Sensors Actuators A: Physical*, vol. 303, 2020, Art. no. 111696.

[12] X. Yang *et al.*, "An in-fiber integrated optofluidic device based on an optical fiber with an inner core," *Lab Chip*, vol. 14, no. 12, pp. 2090–2095, 2014.

[13] O. A. Schmidt, T. G. Euser, and P. S. J. Russell, "Mode-based microparticle conveyor belt in air-filled hollow-core photonic crystal fiber," *Opt. Express*, vol. 21, no. 24, pp. 29383–29391, 2013.

[14] P. Russell, "Photonic crystal fibers," *Science*, vol. 299, no. 5605, pp. 358–362, 2003.

[15] D. K. C. Wu, B. T. Kuhlmey, and B. J. Eggleton, "Ultrasensitive photonic crystal fiber refractive index sensor," *Opt. Lett.*, vol. 34, no. 3, pp. 322–324, 2009.

[16] C. E. Kerbage, B. J. Eggleton, P. S. Westbrook, and R. S. Windeler, "Experimental and scalar beam propagation analysis of an air-silica microstructure fiber," *Opt. Express*, vol. 7, no. 3, pp. 113–122, 2000.

[17] Q. Sun *et al.*, "Graphene-assisted microfiber for optical-power-based temperature sensor," *IEEE Photon. Technol. Lett.*, vol. 28, no. 4, pp. 383–386, Feb. 2015.

[18] L. Li, Q. Han, Y. Chen, T. Liu, and R. Zhang, "An all-fiber optic current sensor based on ferrofluids and multimode interference," *IEEE Sensors J.*, vol. 14, no. 6, pp. 1749–1753, Jun. 2014.

[19] X. Yang *et al.*, "Microfiber interferometer integrated with Au nanorods for an all-fiber phase shifter and switch," *Opt. Lett.*, vol. 44, no. 5, pp. 1092–1095, 2019.

[20] J.-J. Chieh, S.-Y. Yang, H.-E. Horng, C.-Y. Hong, and H.-C. Yang, "Magnetic-fluid optical-fiber modulators via magnetic modulation," *Appl. Phys. Lett.*, vol. 90, no. 13, 2007, Art. no. 133505.

[21] R. M. Morse and H. Feshbach, "Methods of theoretical physics," *Amer. J. Phys.*, vol. 22, no. 12, pp. 5–12, 1953.

[22] H. Kober, *Dictionary of Conformal Representations*. New York, NY, USA: Dover, 1957.

[23] C. Guan, L. Yuan, F. Tian, Q. Dai, and X. Tian, "Mode field analysis of 328 eccentric optical fibers by conformal mapping," in *Proc. 21st Int. Conf. Opt. Fibre Sensors (OFS21). SPIE*, vol. 7753, 77535W, 2011.

[24] C. Y. H. Tsao, D. N. Payne, and L. Li, "Modal propagation characteristics of radially stratified and D-shaped metallic optical fibers," *Appl. Opt.*, vol. 28, no. 3, pp. 588–594, 1989.

[25] C. Tsao, *Optical Fibre Waveguide Analysis*. Oxford, U.K.: Oxford Univ. Press, 1992.